

Jet in Supersonic Crossflow on a Flat Plate

Dean A. Dickmann*

Lockheed Martin Missiles and Fire Control, Grand Prairie, Texas, 75051

and

Frank K. Lu†

University of Texas at Arlington, Arlington, Texas 76019

A three dimensional full Navier-Stokes CFD model with the Smith $\kappa\text{-}\kappa$ turbulence model is used to compute the interaction between a transverse jet and a supersonic crossflow. A new flow model for jets in supersonic crossflow is presented. Details of shock structure, vortex origination and separation/reattachment zones are described. Amplification coefficients are defined and calculated to quantify the obstruction component of the jet interaction forces and moments. The amplification coefficients increase nearly linear with freestream Mach number.

Nomenclature

a	= speed of sound	Re_θ	= Reynolds number based on momentum thickness, $\frac{\rho_e U_e \theta}{\mu_e}$
C_f	= local skin friction coefficient = τ_w/q_∞	S	= area
C_m	= pitching moment coefficient	T	= temperature
C_N	= normal force coefficient	u^+	= $\sqrt{\frac{2}{C_{fw}} \frac{T_\delta}{(T_w - T_\delta)}} \sin^{-1} \left(\frac{u}{u_\delta} \sqrt{1 - \frac{T_\delta}{T_w}} \right)$
C_p	= pressure coefficient	U	= velocity magnitude, = $(u^2 + v^2 + w^2)^{1/2}$
C_T	= thrust coefficient, = $F/(q_\infty S_{ref})$	x	= streamwise Cartesian coordinate
C_1	= Sutherland viscosity constant	y	= normal direction
C_2	= 110 K (198.6 °R)	y^+	= $\frac{p_w \gamma u_\delta (T_w + C_2)}{R_g T_w C_1 T_w^{1.5}} \sqrt{\frac{T_w C_{fw}}{T_\delta 2}}$
e	= internal energy	z	= spanwise direction
l, L	= length	γ	= ratio of specific heats
M	= Mach number	ε	= amplification coefficient
p	= pressure	η	= $\frac{y}{x} \sqrt{\frac{\rho_\infty u_\infty x}{\mu_\infty}}$
Pr	= Prandtl number	κ	= turbulent kinetic energy
		μ	= viscosity

* Senior Staff Engineer, Systems Engineering Department.

† Professor and Director, Aerodynamics Research Center, Mechanical and Aerospace Engineering Department, Box 19018. Associate Fellow AIAA.

q_∞	= dynamic pressure, $= \frac{1}{2} \gamma_\infty p_\infty M_\infty^2$	ρ	= density
R	= gas constant	τ	= shear stress
Re	= Reynolds number	θ	= momentum thickness
Subscripts		LE	= leading edge
a	= computational cell	ref	= reference, namely, user-defined incoming free-stream conditions
bc	= boundary condition	t	= total
g	= gas specific	w	= wall
int	= interior	tf	= transformed

I. Introduction

JETS issuing perpendicularly into a free-stream have been the subject of research for more than 60 years.¹ Much of the research has been focused on vertical/short take off and landing, applications where the free-stream is either quiescent or can be regarded as incompressible. However, some studies have focused on supersonic free-streams. Such normal jets issuing into a supersonic free-stream have been suggested as viable means for aerodynamic vehicular control. Of interest in aerodynamic control is the surface pressure affects of the jet, often referred to as jet interaction or JI. However, a jet issuing perpendicularly into a supersonic flow results in a complex flowfield that makes it difficult to quantify its effect on forces and moments. In the past, some researchers²⁻⁴ have suggested that the jet can be properly represented by a solid cylinder of given transverse length in inviscid flow, but data have shown that this is not a realistic representation. Such a model does not include plume expansion into the free-stream, plume overexpansion downstream or the horseshoe vortex surrounding the jet around the jet exit. Subsequently, Champigny and Lacau⁵ gave a detailed explanation of the flow phenomena present in a jet in supersonic cross-flow. Their flow structure model is shown in Fig. 1.

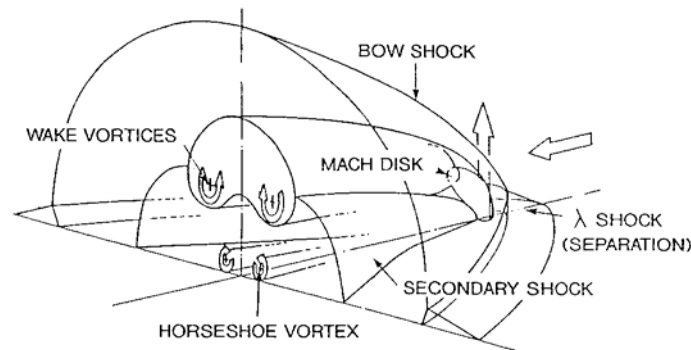


Figure 1. Champigny and Lacau flow structure model.⁵

The Champigny–Lacau model has found widespread acceptance currently. Amongst the flow features is a single upstream separation zone created from a bow shock interaction with the approaching boundary layer. This shock/boundary layer interaction also generates a λ shock, or separation shock. As the jet exits, it initially expands into the crossflow, but turns downstream because of this interaction and a shock forms around the jet, typically referred to as the barrel shock. The barrel shock is terminated with a Mach disk and wake vortices are generated as the plume moves downstream. A secondary shock is formed aft of the jet plume with the so-called horseshoe vortices moving downstream along the surface. The Champigny–Lacau model describes the horseshoe vortex as originating from the boundary layer separation upstream of the jet between the λ -shock region. The present study examines this near field mean flow structure and their effects on forces and moments.

Since there is practical interest in the forces and moments developed, it will be useful to examine the surface pressure arising from JI. An example of the centerline surface pressure for a jet in supersonic cross-flow is shown in Figure 2. The first pressure rise upstream of the jet is induced by the forward leg of the λ -shock structure. Beneath this λ -shock structure is the first (or primary) three-dimensional separation zone which sweeps around both sides of the jet, see Fig. 1. The characteristic shape of this part of the pressure distribution, with a dip and a subsequent large pressure rise, indicates that this separation region is an open type with a strong vertical flow. The second, much higher pressure peak is associated with a stagnation region upstream of the jet. Experimental difficulties prevent surface pressures to be obtained close to the jet opening. The centerline surface pressures aft of the jet indicate an overexpansion and recovery process.

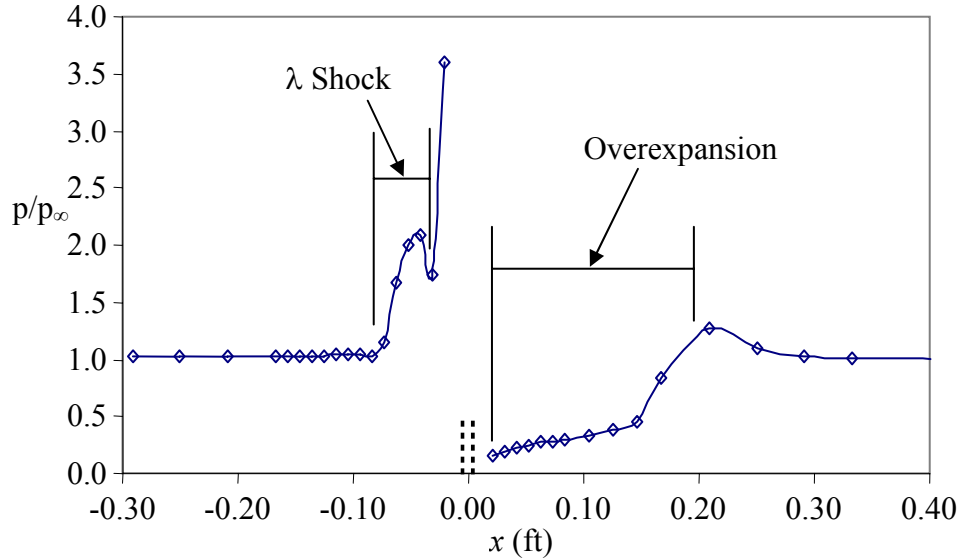


Figure 2. Pressure distribution on centerline of a flat plate with circular jet⁶.

The λ shock region and the over-expanded region are apparent in Fig. 2. Together, these regions are referred to as the obstruction component of JI. The influence of the vortices on downstream surfaces is referred to as the washout component. This paper considers only the obstruction component, but notes the details near the jet causing the formation of the vortices responsible for the washout component.

II. Flow Field Analysis Model

Falcon, a 3-D full Navier-Stokes solver developed by Lockheed Martin, was used with the Smith $\kappa - \kappa \ell$ turbulence model⁷ to simulate a Mach 2.61 flow over a flat plate with a jet and several cases of flow over a flat plate. These results were compared with the Dowdy and Newton⁶ data. The $k-k_l$ model is a two equation model using an equation for the turbulent kinetic energy and another for the product of turbulent kinetic energy and the turbulent length scale. Falcon solves the full set of the unsteady three-dimensional, Favre-averaged conservation equations⁸. Although a steady flow field is expected, the unsteady form of the equations is used because they are a mixed set of hyperbolic and parabolic partial differential equations and the solution techniques for these types of PDEs are compatible. The unsteady equations are marched in time (or pseudo-time) to a steady solution. Falcon allows the user to define a constant Courant-Freidrichs-Lewy (CFL) number, which is a relationship between the time step and the grid mesh size. The limits on this relationship are driven by the stability of the numerical scheme employed to solve the conservations equations. For a constant CFL number, the time step for each cell is different. This effectively warps time between cells throughout the mesh and is acceptable as long as a steady state solution is reached. Solutions that have not reached steady state when a constant CFL is used are physically unrealistic.

II.1 Boundary Conditions

For the no-jet simulations, that is, for flow past a flat plate at zero incidence, user-defined free-stream conditions were used as the initial condition. Figure 3 shows the boundary conditions used in Falcon. At the inflow boundary,

all of the primitive variables, namely, $\rho, \rho u, \rho v, \rho w, \rho e$, are specified. At the outflow boundary, none of the primitive variables are specified. Their values are copied directly from the first interior point, the so-called zeroth-order extrapolation. The far field boundary consists of four parts and is based on a one-dimensional approximation of the inviscid flow equations in characteristic form. Falcon determines if the flow is entering or leaving the boundary and whether it is subsonic or supersonic. For supersonic outflow, all primitive variables are extrapolated from interior points by zeroth-order extrapolation. For supersonic inflow, all of the primitive variables are taken from the user-defined free-stream conditions. Since this study is only concerned with supersonic flow, there is no need to describe this boundary condition for subsonic flow.

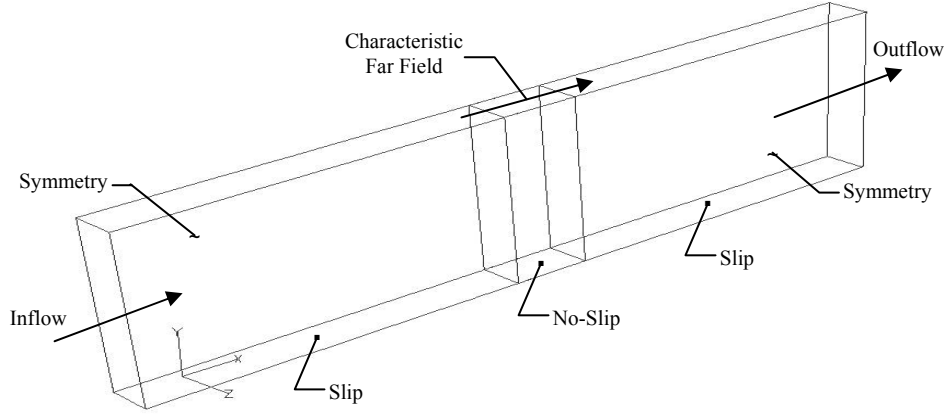


Figure 3. Flat plate boundary conditions.

The slip boundary is also based on the one-dimensional approximation of the inviscid equations and specifies the primitive variables as follows,

$$\rho_{bc} = \rho_{\text{int}} + \frac{p_{bc} - p_{\text{int}}}{a_{\text{ref}}^2} \quad (1)$$

$$e_{bc} = \frac{p_{bc}}{(\gamma - 1)\rho_{bc}} \quad (2)$$

$$(\rho u)_{bc} = \rho_{bc} \left(u_{\text{int}} - V_a \frac{S_{ax}}{|\vec{S}_a|} \right) \quad (3)$$

$$(\rho v)_{bc} = \rho_{bc} \left(v_{\text{int}} - V_a \frac{S_{ay}}{|\vec{S}_a|} \right) \quad (4)$$

$$(\rho w)_{bc} = \rho_{bc} \left(w_{\text{int}} - V_a \frac{S_{az}}{|\vec{S}_a|} \right) \quad (5)$$

where

$$p_{bc} = p_{\text{int}} - \hat{n}_{bc} \rho_{\text{ref}} a_{\text{ref}} V_a \quad (6)$$

$$V_a = \frac{\vec{V}_{\text{int}} \cdot \vec{S}_a}{|\vec{S}_a|} \quad (7)$$

and the user-defined free-stream conditions are used as reference conditions.

A zeroth-order extrapolation is applied to pressure and temperature for the adiabatic, no-slip wall. Since Smith's turbulence model is used, the pressure is modified as follows,

$$p_{bc} = p_{\text{int}} + \frac{1}{3}((\rho k)_{\text{int}} - (\rho k)_{bc}) \quad (8)$$

The primitive variables, $\rho u, \rho v, \rho w$, are set to zero and the internal energy is handled the same as the slip boundary stated above.

For the symmetry boundary, a zeroth-order extrapolation is applied to density and pressure with the velocities determined as follows,

$$(\rho u)_{bc} = (\rho u)_{\text{int}} - \frac{(\rho \vec{V})_{\text{int}} \cdot \vec{S}_a}{|\vec{S}_a|} S_{ax} \quad (9)$$

$$(\rho v)_{bc} = (\rho v)_{\text{int}} - \frac{(\rho \vec{V})_{\text{int}} \cdot \vec{S}_a}{|\vec{S}_a|} S_{ay} \quad (10)$$

$$(\rho w)_{bc} = (\rho w)_{\text{int}} - \frac{(\rho \vec{V})_{\text{int}} \cdot \vec{S}_a}{|\vec{S}_a|} S_{az} \quad (11)$$

and, finally, the internal energy is

$$e_{bc} = e_{\text{int}} - \frac{1}{2} \rho_{\text{int}} |\vec{V}_{\text{int}}|^2 + \frac{1}{2} \rho_{bc} |\vec{V}_{bc}|^2 \quad (12)$$

For the flat plate with a jet, the only additional boundary condition is the boundary at the inlet of the nozzle where total pressure p_t and the total temperature T_t are specified. Falcon assumes that at the linearization or reference point that the following characteristic equation is constant.

$$\frac{\vec{V}_{\text{int}} \cdot \vec{S}_a}{|\vec{S}_a|} + \frac{p_{\text{ref}}}{\rho_{\text{ref}} a_{\text{ref}}} = B \quad (13)$$

Given

$$T_t = T + \frac{\gamma - 1}{2\gamma} \frac{U^2}{R_g} \quad \frac{p}{p_t} = \left(\frac{T}{T_t} \right)^{\gamma/\gamma-1}$$

the following equation results,

$$\frac{2\gamma R_g}{\gamma - 1} T_t \left(\frac{p}{p_t} \right)^{\gamma-1/\gamma} + \left[\left(\frac{p_t}{\rho a} \right)^2 M_\infty^2 \right] \left(\frac{p}{p_t} \right)^2 - 2BM_\infty^2 \frac{p_t}{\rho a} \left(\frac{p}{p_t} \right) + B^2 M_\infty^2 - \frac{2\gamma R_g}{\gamma - 1} T_t = 0$$

This equation is differentiated and solved for p/p_t . Once p is known, T and U can be found from the previous equations. If the user inputs the three components of the velocity vector, they are used to determine a unit vector and U is used as the magnitude of the velocity vector at the boundary.

III. Results and Discussion

III.1 Undisturbed Laminar Boundary Layer

Falcon was used to obtain the undisturbed boundary layer over a flat plate as a preliminary step prior to its use for simulating more complex flows. Figure 4 shows the result for a laminar simulation for an incoming flow at Mach 2 and Mach 4, both at a Reynolds number of 328,000/m. In the figure, the velocity is normalized by the incoming free-stream. The computed profiles were compared against Van Driest's analytical results⁹ Figures 4a and b show velocity profiles at Mach 2 and 4, respectively, at 0.15 and 0.46 m. The computed profiles match those of the theoretical Van Driest profiles very well. The effect of Mach number in thickening the boundary layer is also evident in the figures. Further comparisons between the computations and theory are omitted for brevity.

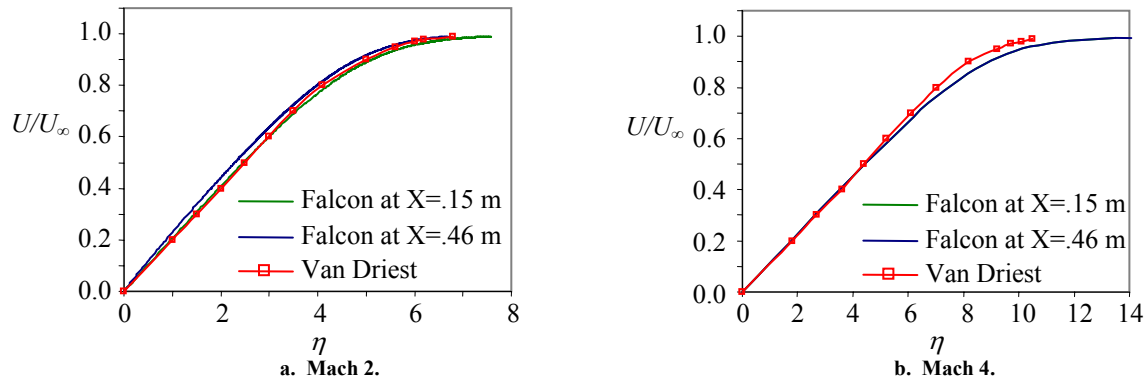


Figure 4. Laminar boundary layer profiles at Mach 2 and Mach 4, both at a Reynolds number of 328,000/m.

III.2 Undisturbed Turbulent Boundary Layer

A further test of Falcon was performed by using it to simulate supersonic turbulent flow past a flat plate. Specifically, it was used to compare against the data of Shutts et al.¹⁰ and Mabey et al.¹¹ as compiled by Fernholz and Finley¹². Figure 5 and 6 show the boundary layer velocity profiles in wall coordinates for both datasets at two locations along the plate compared with the computational results.

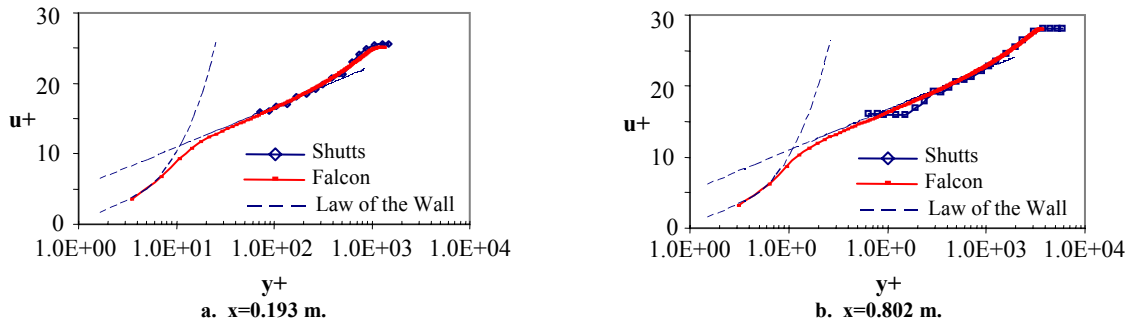


Figure 5. Comparison with Shutts et al.'s data at $M=2.23$, $Re_x=25 \times 10^6/m$.

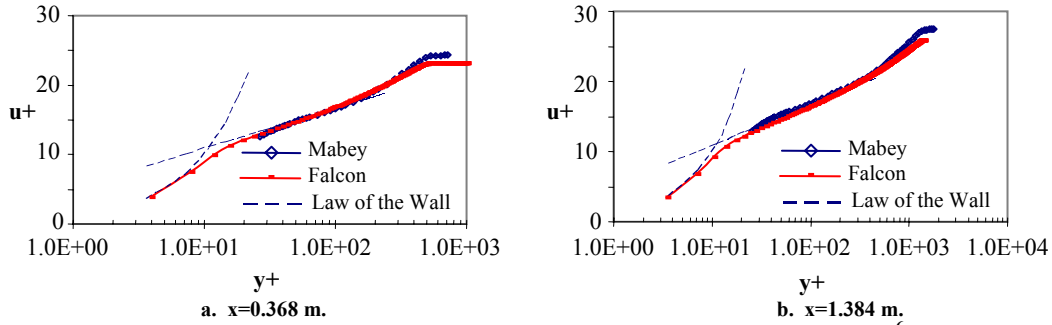


Figure 6. Comparison with Mabey et al.'s data at $M=4.5$, $Re_x=28.1 \times 10^6/m$.

Falcon matches experimental data well at both Mach 2.23 and Mach 4.5 for the logarithmic and wake layers.

Local skin friction coefficients are compared in Figures 7. The Van Driest II (VDII) transformation¹³ of the skin friction coefficient for turbulent compressible flow is used. A summary of the Van Driest II transformation and other skin friction prediction methods can be found in Hopkins and Inouye¹⁴. Hopkins and Inouye recommended this theory and compare it to the Karman-Schoenherr equation (Eq. 3 in Ref. 14). These figures show the transformed test data, the transformed CFD results and the Karman-Schoenherr equation. Falcon compares well at Mach 2.23 but not at 4.5.

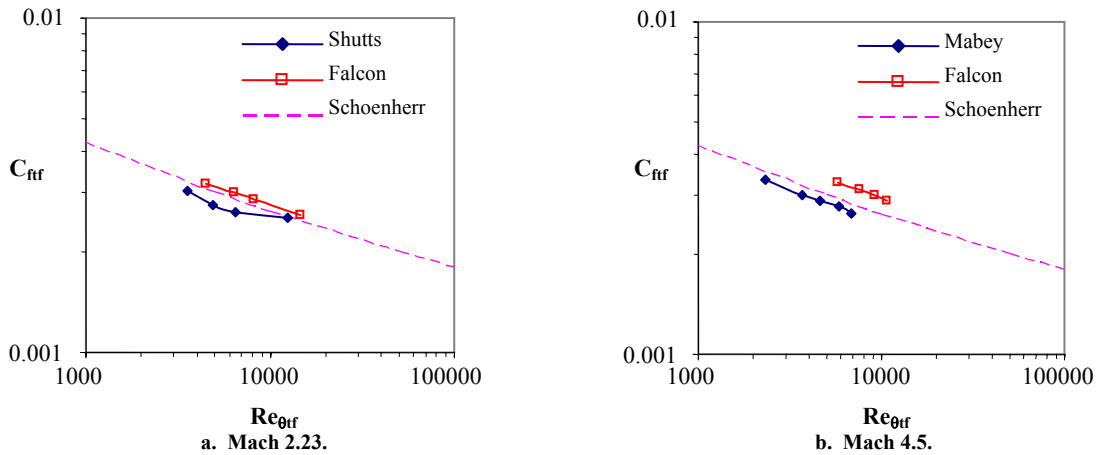


Figure 7. Local skin friction coefficient.

III.3 Transverse Sonic Jet in Supersonic Crossflow With A Turbulent Boundary Layer

In Fig. 8a, velocity vectors are plotted with pressure contours of the upstream flow structure for a simulation of a jet issuing into Mach 2.5 flow while Fig. 8b is a sketch of the salient flow features. These figures show the flow field structure on the symmetry plane ahead of the jet. The underexpanded jet presents an obstruction to the inviscid freestream which adjusts to its presence through a detached bow shock, similar to a cylinder in supersonic crossflow. The inviscid bow shock interacts with the approaching boundary layer creating a complex shock/boundary layer interaction.

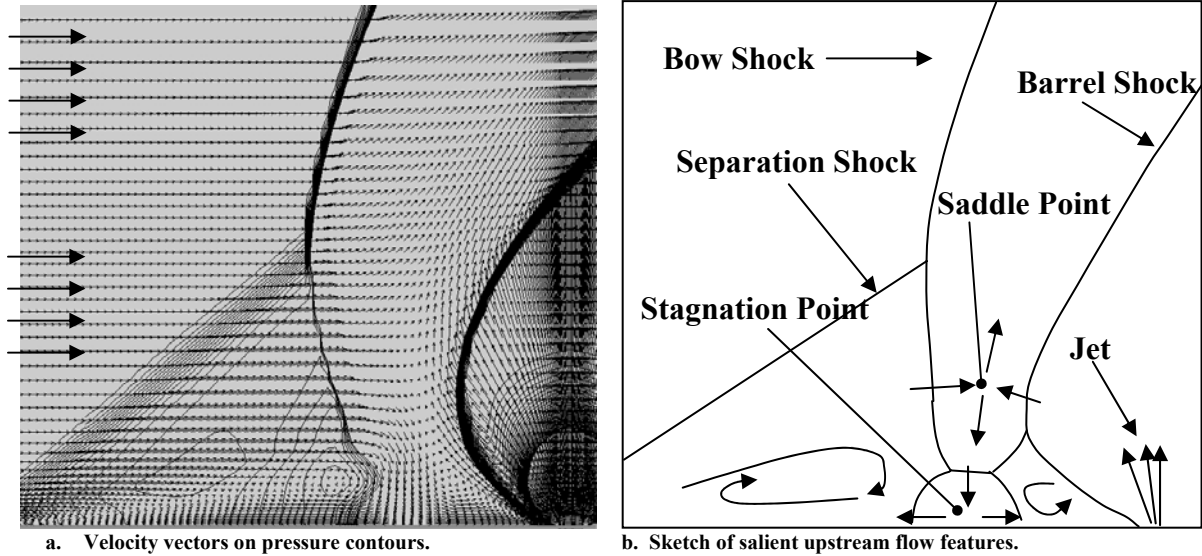


Figure 8. Upstream flow structure.

Further examination shows the jet expands into the freestream and is then turned downstream through a shock, referred to as the barrel shock. Between the shock/boundary layer interaction and the barrel shock is a complex interaction region. In this region, flow from the jet and the freestream approach a saddle point in a nearly horizontal plane and recede from the saddle point in a nearly vertical plane, Fig. 8b. The vertical flow receding from the saddle point accelerates toward the wall to a supersonic Mach number creating a pocket of supersonic flow near the wall in this interaction region. As this flow approaches the wall, a normal shock is formed to adjust the flow to the presence of the wall. After the normal shock, the flow stagnates at the wall. Between this stagnation and barrel shock, a second recirculation is generated through viscous entrainment and pressure distribution. This second recirculation is the origin of the so-called horseshoe vortex. This flow structure has been previously observed by Bowersox¹⁵, however, the saddle point and stagnation region in the interaction region between the shock/boundary layer interaction and the barrel shock have not been previously observed.

A plot of velocity vectors one grid point off the wall is presented in Fig. 9a from the same simulation. This plot is a good representation of the shear stress directions on the surface of the plate, thereby allowing the identification of separation and reattachment lines. Figure 9b is a schematic sketch of the major surface features. It shows the presence of three separation and reattachment zones.

The first separation line, S1, occurs twenty diameters upstream of the jet with the reattachment line, A1, occurring eight diameters upstream. The second separation line, S2, occurs one diameter upstream with its reattachment, A2, occurring 6 diameters upstream. The flow in these primary and secondary separation zones are counter-rotating, as indicated in Fig. 8b. The pressures in this region between S1 and S2 are well above ambient due to the separation shock/boundary layer interaction. This high pressure level helps to amplify the jet thrust. The high pressure along the centerline upstream of the jet produces a transverse pressure gradient in the boundary layer that induces a transverse flow between S1 and A1. The vortical flow between S1 and A1 is not strong enough to persist downstream. The rotating flow within this region dissipates and moves transversely until it meets the first separation shock again and is then realigned with the free-stream. Moreover, the secondary separation zone between S2 and A2 develop into twin counter-rotating vortices with their axes of rotation eventually becoming parallel to the free-stream. These are the so-called horseshoe vortices.

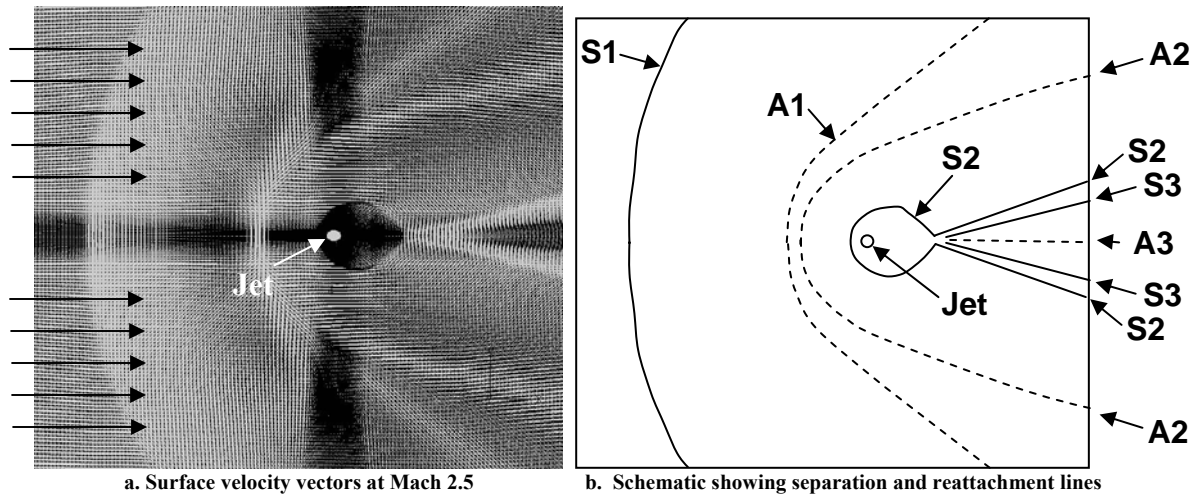


Figure 9. Surface streamlines.

There is one more separation/reattachment pair aft of the jet, S3-A3, but this does not have the same character as S1-A1 because its axis of rotation is never perpendicular to the freestream. As S2 wraps round the jet, it converges on itself at a point aft of the jet. A separation occurs immediately downstream of this point, then the flow reattaches aft of the separation generating the reattachment shock seen in Figure 11a and sketched in 11b. The horseshoe vortices from the secondary separation zone continue propagating downstream in a path modified by this downstream reattachment shock. The transverse pressure gradient induces two mirrored separation zones between S3-A3.

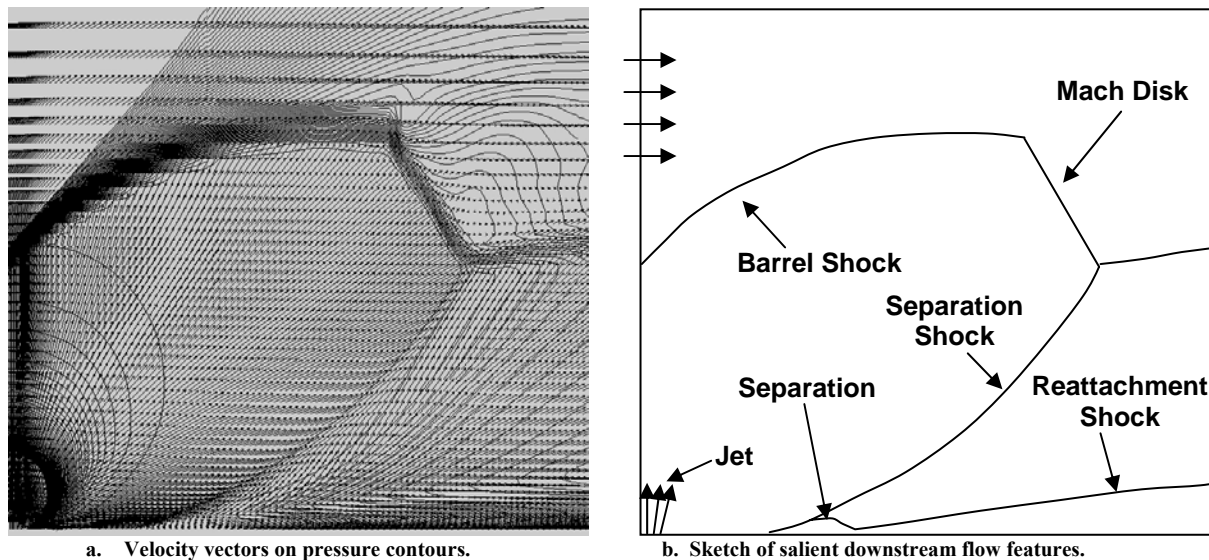


Figure 11. Mach disk location.

Twin vortices within the S3/A3 zones are the dominant mechanisms for modifying the surface pressures on downstream lifting surfaces such as wings and control fins, the so-called washout component of JI.

The vortices originating from the upstream separation and the jet overexpansion produce a large region of sub-ambient pressure aft of the jet. A key component in attenuating the jet thrust in the near field, the so-called obstruction component. As shown in Figure 14, this region persists for 50 diameters downstream, $2 \frac{1}{2}$ times longer than the upstream shock structure region.

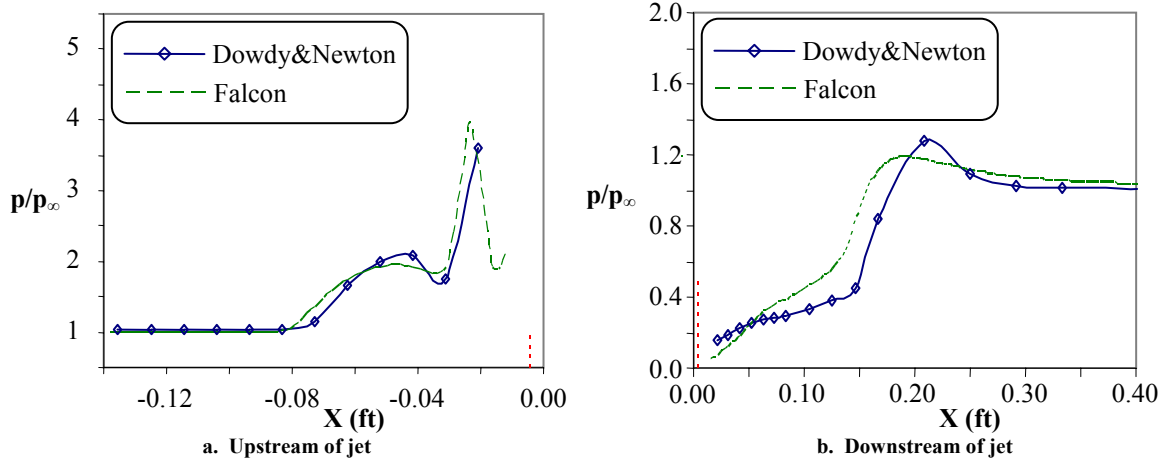


Figure 12. Surface pressure along the centerline

Figures 12a and 12b show the resulting centerline pressure distributions upstream and downstream of the jet from Falcon match experimental data⁶ well. With the results from Falcon verified, the solver is applied to the flat plate with a jet in crossflows of varying Mach numbers. Figure 13 and 14 show the centerline pressure distribution for each of these cases upstream and downstream of the jet, respectively. All of the upstream pressure distributions exhibit similar characteristics with a pressure plateau, a peak pressure followed by an expansion, a small pressure rise and finally a thin region of overexpansion, however two trends can be seen in Figure 13. As Mach increases, the peak pressure increases and moves downstream. Additionally, the initial pressure rise leading to the pressure plateau moves downstream as Mach increases, but settles to a single location for Mach greater than 3.0. This characteristic is similar to the hypersonic limit seen in detached shocks on blunted bodies.

The downstream pressure distributions exhibit similar characteristics as well, Figure 14. An initial large overexpansion followed by a pressure rise to a pseudo-plateau, then a second pressure rise until it overshoots ambient pressure and finally an expansion to ambient. As Mach increases, the overshoot decreases in magnitude and the overshoot peak moves upstream.

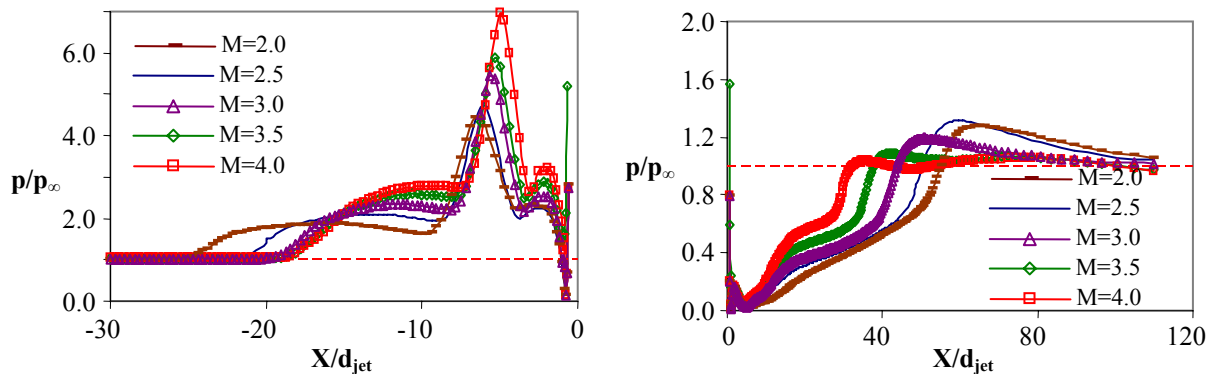


Figure 13. Upstream Centerline Pressure Distributions. Figure 14. Downstream Centerline Pressure Distributions.

Given these pressure distribution, characteristic lengths can be defined. The length of the influence upstream of the jet can be defined as the distance between the initial pressure rise to the edge of the jet exit. The length of the influence downstream of the jet can be defined as the distance between the point at which the pressure first meets ambient pressure to the edge of the jet exit. Figure 15 show these lengths nondimensionalized by the jet diameter as a function of Mach. The upstream length asymptotically approaches a constant value while the downstream length varies linearly with Mach.

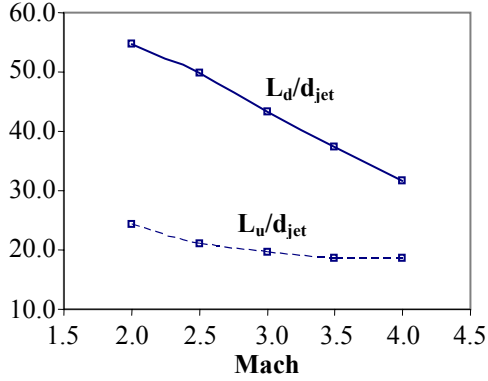


Figure 15. Upstream and Downstream Characteristic Jet Influence Lengths.

Since the jet is intended to produce a force to move the plate, it would be useful to integrate the surface pressures and determine if the low pressure downstream of the jet is strong enough to attenuate the high-pressure region and the jet thrust. Amplification coefficients, defined as,

$$\varepsilon_{m_jet} = \frac{C_{m_LE}}{C_T \frac{L_{jet}}{L_{ref}}} \quad \varepsilon_{N_jet} = \frac{C_N}{C_T}$$

are used to quantify the JI effect. A coefficient of 1.0 shows no amplification or attenuation, greater than 1.0 indicates amplification and less than 1.0 indicates attenuation. Figure 16 presents the amplification coefficients as a function of Mach number.

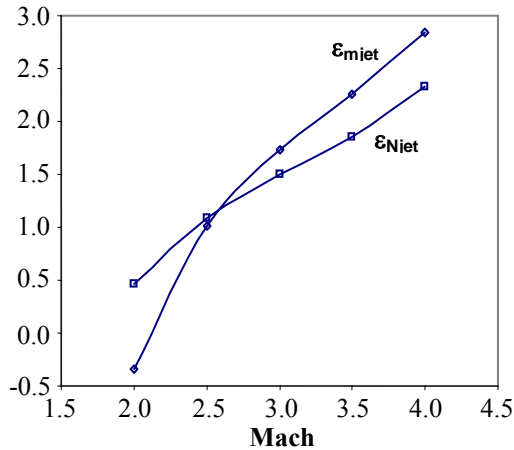


Figure 16. Amplification coefficients.

The amplification factors are linear with a break point in their slopes at approximately Mach 2.5. Over the entire Mach range considered, the amplification coefficients indicate force and moment amplification by JI, $\varepsilon > 1.0$, except at Mach numbers below 2.5. Below 2.5, the amplification coefficients indicate attenuate of the force and moment, $\varepsilon < 1.0$. The moment amplification coefficient is negative below approximately 2.1. This indicates a moment reversal. Extrapolation of the normal force data to lower Mach numbers suggests it would reverse direction as well.

IV. Conclusions

A new, more complete flow model for jets in supersonic cross-flow has been described. A saddle point and stagnation point upstream of the jet are described as well as a downstream reattachment shock. The complicated nature of transverse jets in supersonic crossflow, TJICF, requires the full set of Navier-Stokes with an adequate turbulence model for examination. The obstruction component of the force and moment are amplified over the Mach range considered except for the moment at Mach numbers below 2.5 where it is attenuated. The amplification factors are linear with Mach number, but both the force and moment amplification factors have a break point at approximately Mach 2.5. Below Mach 2.1, the moment is not only attenuated, it also changes direction.

V. References

1. Margason, R.J., "Fifty Years of Jet in Cross Flow Research," AGARD 72nd FDP Meeting, Paper No. 1, 1993.
2. Ferrari, C., "Interference Between a Jet Issuing Laterally from a Body and the Enveloping Supersonic Stream," JPL Bumblebee Series, Report No. 286, April 1959.
3. Spaid, F.W., "A Study of Secondary Injection of Gases into a Supersonic Flow," Ph.D. Dissertation, California Institute of Technology, 1964.
4. Spaid, F.W. and Cassel, L.A., "Aerodynamics Interference Induced by Reaction Controls," AGARDograph No. 173, Dec 1973.
5. Champigny, P. and Lacau, R.G., "Lateral Jet Control For Tactical Missiles," Special Course On Missile Aerodynamics, AGARD-R-804, Paper No. 3, 1994.
6. Dowdy, M.W. and Newton, J.F., "Investigation of Liquid and Gaseous Secondary Injection Phenomena on a Flat Plate with $M = 2.01$ to $M = 4.54$," JPL-TR-32-542, Dec. 1963.
7. Smith, B.R., "The $k-k_l$ Turbulence Model and Wall Layer Model for Compressible Flows," AIAA Paper 90-1483, June 1990.
8. Wilcox, D.C., *Turbulence Modeling for CFD*, DCW Industries, La Cañada, California, 2nd ed., 1998.
9. Van Driest, E.R., "Investigation of Laminar Boundary Layers in Compressible Fluids Using the Crocco Method," NACA-TN-2597, Jan. 1952.
10. Shutts, W.H., Hartwig, W.H. and Weiler, J.E., "Final Report On Turbulent Boundary Layer And Skin Friction Measurements on a Smooth, Thermally Insulated Flat Plate at Supersonic Speeds," University of Texas, Defense Research Laboratory Report 364, 1955.
11. Mabey, D.G., Meier, H.U. and Sawyer, W.G., "Experimental and Theoretical Studies of the Boundary Layer on a Flat Plate at Mach Numbers from 2.5 to 4.5," RAE TR 74127, 1974.
12. Fernholtz, H.H. and Finley, P.J., "A Critical Compilation of Compressible Turbulent Boundary Layer Data," AGARDograph No. 223, June 1977.
13. Van Driest, E.R., "Problem of Aerodynamic Heating," *Aeronautical Engineering Review*, Vol. 15, No. 10, Oct. 1956, pp. 26-41.
14. Hopkins, E.J. and Inouye, M., "An Evaluation of Theories for Predicting Turbulent Skin Friction and Heat Transfer on Flat Plates at Supersonic and Hypersonic Mach Number," *AIAA Journal*, Vol. 9, No. 6., pp. 993-1003, June 1971.
15. Mahmud, Z. and Bowersox, R.D.W., "Aerodynamics of Low-Blowing-Ratio Fuselage Injection into a Supersonic Freestream," *Journal of Spacecraft and Rockets*, Vol. 42, No. 1, pp. 30-37, Jan 2005.